Appl. Phys. B 62, 263–272 (1996)

Applied Physics B Lasers and Optics

Infrared absorption of silane, ammonia, acetylene and diborane in the range of the CO_2 laser emission lines: Measurements and modelling

J. Förster[1], Th. Hagen[1], M. von Hoesslin[1], J. Uhlenbusch[1,2]

[1] Institut für Laser- und Plasmaphysik, Heinrich-Heine-Universität Düsseldorf, D-40225, Düsseldorf, Germany
(Fax: + 49-211/311-3718, E-mail: UHLENB@convex.rz.uni-duesseldorf.de)
[2] Institut für Plasmaphysik, Forschungszentrum Jülich GmbH, D-52425 Jülich, Germany

Received: 24 April 1995/Accepted: 28 August 1995

Abstract. Absorption spectra of the gases SiH_4, NH_3, C_2H_2 and of SiH_4/Ar and SiH_4/B_2H_6 mixtures have been measured in the spectral range of the CO_2 laser from 9.2 to 10.8 μm. In agreement with literature, silane shows the highest absorption (absorption coefficient $\alpha = 3.3 \times 10^{-2}$ $Pa^{-1}\,m^{-1}$). The deviation of the measured absorption behaviour of silane from literature, as far as the pressure dependence is concerned, can be explained by the enhanced spectral energy density in our experiment. This is confirmed by a rate-equation model involving the basic mechanisms of V–V and V–T energy transfer between vibrationally excited silane molecules. In contrast to silane, the absorption coefficient α of NH_3 at the $10P(20)$ laser line is 4.5×10^{-4} $Pa^{-1}\,m^{-1}$ at $p = 20$ kPa and has its maximum of 4.5×10^{-3} $Pa^{-1}\,m^{-1}$ at the $10R(6)$ laser line. For C_2H_2 and B_2H_6, α is even less ($\leq 2.1 \times 10^{-5}$ $Pa^{-1}\,m^{-1}$ for C_2H_2).

PACS: 33.20; 34.50

Nowadays, IR-laser-induced chemical processes are of growing importance for several applications, such as semiconductor production, surface treatment in material sciences, production of superconducting films, and synthesis of ultrafine powders which can be processed to high-quality ceramics. The powder synthesis (by the method of laser-induced pyrolysis) is subject of research in our institute, whose results are presented in detail elsewhere [1–3]. In all cases mentioned in literature, mainly the $10P(20)$ line at $\lambda = 10.591$ μm of a CO_2 laser is used, whose absorption behaviour is well known for most gases of laser chemical interest.

Haggerty and Cannon [4] measured $\alpha(\lambda)$ of SiH_4 and NH_3 also for other CO_2 laser wavelengths. However, the spectral energy density of their laser system (10^{-12} Jsm^{-3}) was two orders of magnitude smaller than that in our experiments, making the mere adaptation of their data to our experimental conditions questionable. Additional absorption data, which can be extracted from literature, mainly result from experiments concerning small-signal absorption (linear absorption), as given for C_2H_4, NH_3, and O_3 in [5], for B_2H_6 in [6], and for triethylborane in [7], or concerning multiple-photon IR absorption, as given in [8–12]. Both cases are different to the measurements presented in this work, where pressures of 50 kPa are combined with spectral energy densities in the order of 10^{-10} Jsm^{-3}. These high values correspond to the experimental conditions of our laser-induced pyrolysis setup, possessing gas-to-powder conversion efficiencies of more than 95 %. The fact that for our experimental conditions only sparse information on the absorption of the reactant gases is available leaded to the investigations reported in the following for SiH_4, NH_3, C_2H_2, as well as for SiH_4/Ar and SiH_4/B_2H_6 mixtures.

1 Experimental setup

A schematic sketch of the absorption setup can be seen in Fig. 1. The CO_2 laser beam is split into a signal beam and a reference beam, both beams being chopped mechanically with different frequencies. Two light barriers record synchronously lock-in times of the chopper for each channel, while the power supply of the chopper controls its rotation and the light barrier signals. The signal beam transmitted through the ZnSe windows of the the absorption chamber is attenuated to the sensitivity range of the pyroelectric detector 1. The modular mechanical setup of the absorption chamber allows to adjust different absorption path lengths between 2 and 32 cm. The intensity of the reference beam is also reduced by an attenuator and led to the pyroelectric detector 2. The leakage rate of the absorption chamber was better than 2×10^{-7} Pam^3s^{-1}.

The output signals of detector 1 and 2 and of the chopper are connected to two separate lock-in amplifiers. After filtering the lock-in output, signals are led to a ratiometer, where a signal which is proportional to the ratio of the two lock-in signals is generated. This is plugged into one channel of the x-y-plotter. The other channel is fed by a signal proportional to the pressure in the absorption chamber.

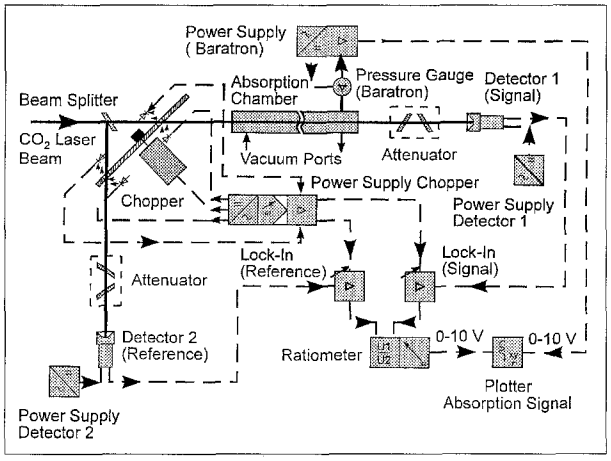

Fig. 1. Scheme of the absorption setup

2 Experimental results

In this section, measured absorption data for SiH_4, NH_3, C_2H_2, SiH_4/Ar and SiH_4/B_2H_6 mixtures at room temperature in the pressure regime from 0 to 100 kPa are presented. The experimental parameters summarized in Table 1 are common for all measurements.

Before each measurement, both axes of the *x*-*y*-plotter were calibrated by exposing the reference lock-in to a well-defined chamber pressure and exposing the ratiometer to a well-defined attenuation. After tuning the CO_2 laser to a new line, the absorption chamber was evacuated and the corresponding absorption value arbitrarily set zero. Then, the chamber was slowly filled with the gas under investigation (rate of pressure increase 0.1–0.5 kPa/s), and the absorption was measured for different pressures. The procedure was repeated for the next CO_2 laser line. The measurements on silane, ammonia, and the silane/diborane mixture were performed with the minimum chamber length of 2 cm, whereas for the measurements at C_2H_2 the maximum chamber length of 32 cm was used.

The measured curves were evaluated by means of the integral Lambert-Beer law:

$$I = I_0 \exp(-\alpha d), \tag{1}$$

giving for the absorption coefficient α:

$$\alpha = \frac{\ln\left(\frac{I_0}{I}\right)}{pd} \tag{2}$$

with the absorption length d, gas pressure p, and laser intensities in the signal and the reference branch I and I_0, respectively.

2.1 Silane and silane/argon mixtures

In Fig. 2, the absorption coefficient for silane is shown, as determined from measurements at the $10P(20)$ laser line and $p = 0$–20 kPa. After a steep increase of the α value vs pressure until $p = 1.5$ kPa, a moderate increase (approximately linear) up to $\alpha = 3.2 \times 10^{-2}$ $Pa^{-1}m^{-1}$ at $p = 20$ kPa is observed. This behaviour remarkably differs from the measurements of Haggerty and Cannon [4], which should be discussed in the following. Their absorption setup is quite similar to the equipment employed here, whereas the CO_2 laser devices are different. The laser used by Haggerty and Cannon had a repetition rate of 1 Hz, pulse duration of 1 ms and a pulse energy of 100 mJ, giving an average power of only $P_{av} = 0.1$ W. According to the following relation

$$\varrho_{Ph} = \frac{I_L}{c\Delta\nu_{Laser}} = \frac{P_{av}}{c\pi(3w_0/2)^2\Delta\nu_{Laser}} \tag{3}$$

Table 1. Experimental parameters of the absorption measurements

Experimental conditions	
CO_2 laser	
Total gas flow	$\dot{V} = 0.2$ Nm^3h^{-1}
Gas mixture	$\dot{V}_{He}:\dot{V}_{N_2}:\dot{V}_{CO_2} = 82:13.5:4.5$
Discharge pressure	$p = 10$ mbar
Discharge current	$I = 70$ mA
Width of gain profile	$\delta\nu_V \approx 60$ MHz
Dominant broadening mechanism	Doppler
Transversal mode	TEM_{00}
Longitudinal mode distance	$\delta\nu_{Laser} = 26$ MHz
Spectral width of emission line	$\Delta\nu_{Laser} = 1.5$ MHz
Frequency stability	≈ 10 MHz
Average laser power	$P_L = 25$ W
Beam diameter	$3w_0 = 18$ mm
Spectral energy density	$\varrho_{Ph} \approx 10^{-10}$ J s m^{-3}
Absorption chamber	
Absorption length	$d = 2$–32 cm (see text)
Diameter of absorption chamber	$D = 36$ mm
Average laser power	$P_{av} = 10$ W
Chopper	
Modulation frequency (reference)	$f_r = 80$ Hz
Modulation frequency (signal)	$f_a = 64$ Hz

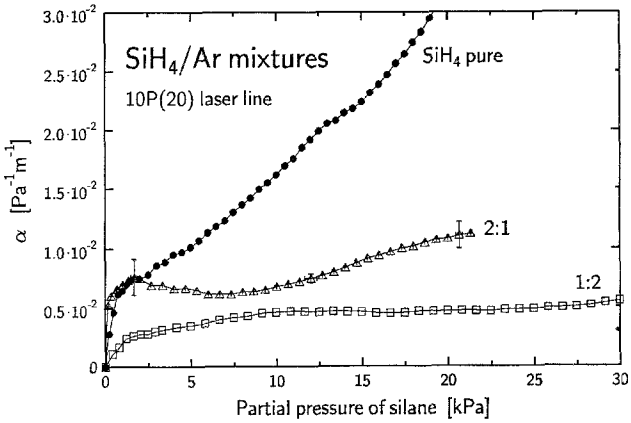

Fig. 2. Measured absorption coefficient α for silane and silane/argon mixtures vs partial pressure of silane

for the spectral energy density ϱ_{Ph} of the laser, the measurements presented in this work correspond to a value of ϱ_{Ph} about a factor 100 higher than in the case of Haggerty and Cannon [4]. The spectral widths of the lasers $\Delta\nu_{Laser}$ and their beam diameters w_0 are assumed to be similar. The high spectral energy density causes a considerable alteration of the population density, as is shown below.

Further absorption experiments were performed with SiH_4/Ar mixtures at the same laser line ($\lambda = 10.591$ µm). Figure 2 furthermore presents the p-dependence of the absorption coefficient for pure silane, a 2:1, and a 1:2 mixture of SiH_4 and argon. Two features are obvious: first, the strong decrease of α when the argon concentration is raised at a constant silane partial pressure. On the other side, α keeps constant or is even higher for a stronger dilution with argon. These experiments show that measurements at pure gases do not necessarily allow conclusions for the pyrolysis process in a mixture of gases.

Besides the $10P(20)$ transition, the absorption coefficient vs pressure was also measured for a variety of CO_2 laser wavelengths. Examples are given in Fig. 3 for $p = 2.5$ kPa and $p = 50$ kPa. As can be seen, for $p = 2.5$ kPa, the strongest absorption occurs on the $10P(20)$ line with $\alpha = 8.2 \times 10^{-3}$ Pa^{-1} m^{-1}. Further lines with similar high absorption coefficients are $10P(24)$, $10P(36)$, and $10R(12)$. In the 9 µm regime, only weak absorption is observed, corresponding to α values one order of magnitude lower than the $10P(20)$ data. With increasing pressure, the absorption in the 10 µm regime becomes too high to allow precise determination even in the case of minimum absorption chamber length ($d = 2$ cm), leading to peaks which surpass the upper edge of the diagram (as in Fig. 3 for $p = 50$ kPa). But also peaks with a different behaviour were recorded, as the line $10R(12)$, showing a decrease of α from 7.5×10^{-3} Pa^{-1} m^{-1} at $p = 2.5$ kPa to 3.7×10^{-3} Pa^{-1} m^{-1} at $p = 50$ kPa. In the 9 µm regime up to $p = 50$ kPa, no significant raise of the absorption was measured.

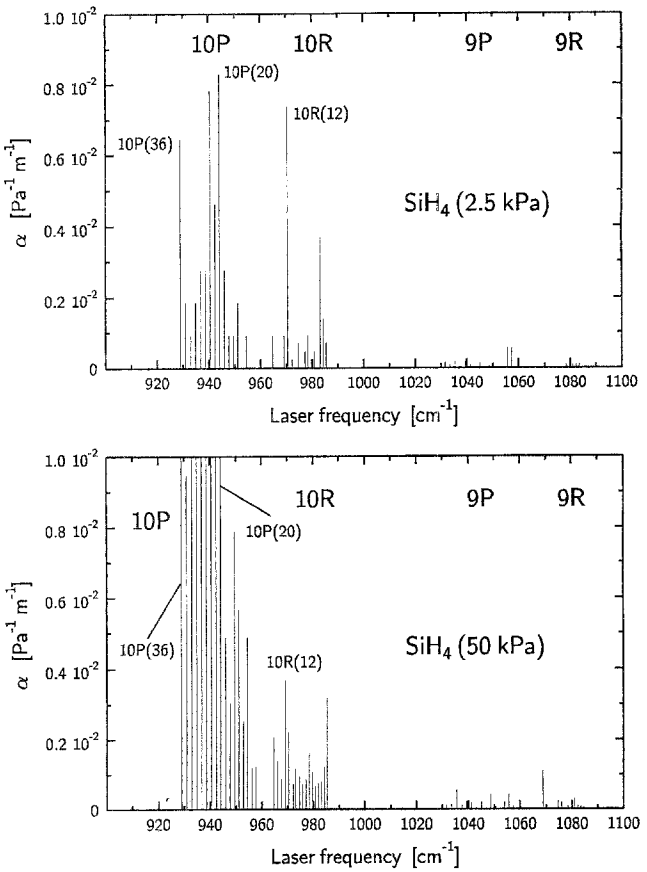

Fig. 3. Synopsis of the absorption coefficient α for silane for various laser frequencies

2.2 Silane/diborane mixture

Absorption experiments with a SiH_4/B_2H_6 mixture (2:3), which were started around the $10P(30)$ transition, yielded no reasonable data because even the moderate laser power of 10 W induced massive chemical reactions in the absorption chamber. These reactions lead to a coating of the ZnSe windows, which had to be entirely cleaned before the next experimental run could be performed. Nevertheless, it could be concluded, that the absorption of B_2H_6 is only weak in contrast to that of silane. Also for the $10P(20)$ line, it showed to be negligible, which is in agreement with literature [6].

2.3 Ammonia

The experiments with ammonia were performed under the same experimental conditions as for silane, also showing a strong pressure dependence for this gas. As can be seen from Fig. 4 for the $10P(20)$ line, α has a clear maximum in the region below $p = 5$ kPa. For pressures $p > 40$ kPa, α remains nearly constant ($\approx 4 \times 10^{-4}$ Pa^{-1} m^{-1}). This behaviour is confirmed by the measurements of Haggerty and Cannon [4]. The fact that an increase of ϱ_{Ph} by two orders of magnitude does not change the absorption behaviour leads to the conclusion that the energy transfer to the ammonia molecule is mainly realized by interaction with other molecular species (collisions).

For other CO_2 laser wavelengths, the pressure dependence of α was also investigated. Figure 5 shows the

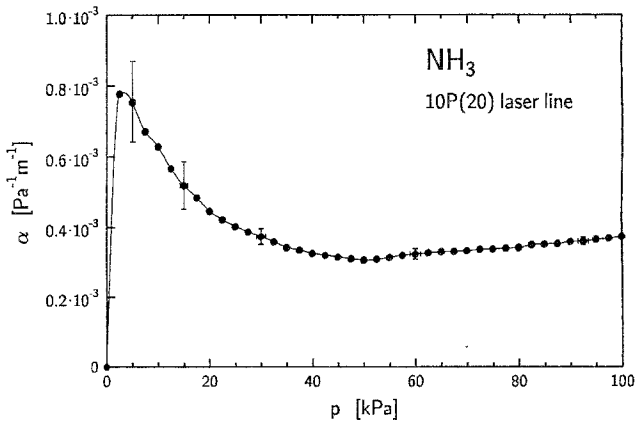

Fig. 4. Absorption coefficient α for ammonia vs pressure p

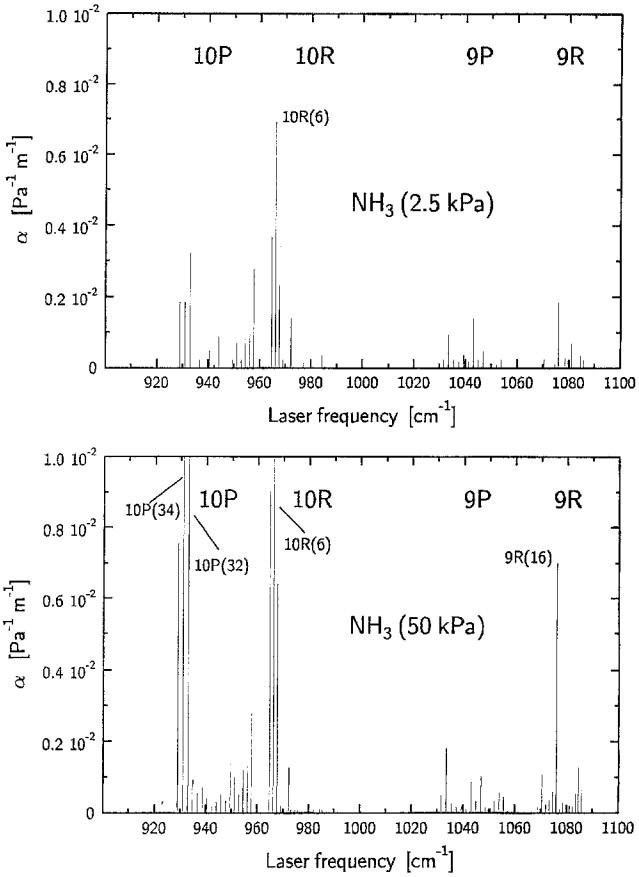

Fig. 5. Synopsis of the absorption coefficient for ammonia for various laser frequencies

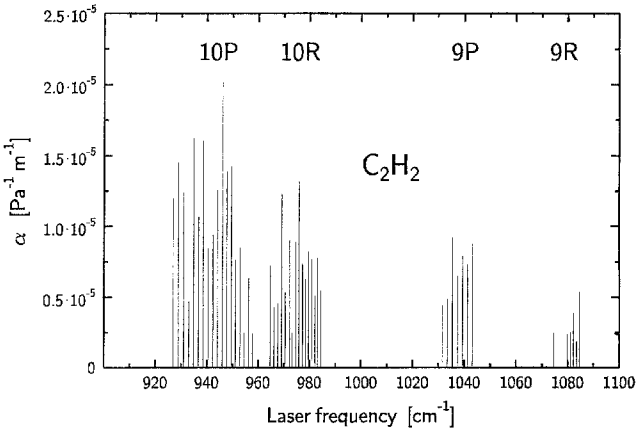

Fig. 6. Synopsis of the absorption coefficient α for acetylene for various laser frequencies

spectral behaviour of α for $p = 2.5$ kPa and $p = 50$ kPa. At low pressure, only few lines reach a value of $2\text{–}4 \times 10^{-3}$ Pa^{-1} m^{-1}, with the exception of the transition $10R(6)$ attaining 7×10^{-3} Pa^{-1} m^{-1}. At this position of the CO_2 laser spectrum [as well as for $10P(32)$ and $10P(34)$], α can be raised to more than 10^{-2} Pa^{-1} m^{-1} by increasing p to 50 kPa, whereas the absorption at $10P(20)$ remains small for this pressure (3.1×10^{-4} Pa^{-1} m^{-1}). With exception of the line $9R(16)$, where α grows until 7.0×10^{-3} Pa^{-1} m^{-1} at $p = 50$ kPa, α is not a function of pressure in the 9 μm regime. A similar result was found for silane. The corresponding values of the absorption coefficient of ammonia are less than 2×10^{-3} Pa^{-1} m^{-1}.

2.4 Acetylene

In contrast to SiH_4 and NH_3, the absorption coefficient of C_2H_2 is nearly constant over the whole pressure range from 0 to 100 kPa. Therefore, only the spectral behaviour of the absorption (for an absorption length $d = 32$ cm) is given in Fig. 6. The absorption coefficient α is comparatively very low for every CO_2 laser wavelength and reaches its maximum value of 2.1×10^{-5} Pa^{-1} m^{-1} at the $10P(18)$ line.

3 Modelling the CO_2 laser line absorption by the silane molecule

Silane is a tetrahedral molecule which belongs to the pointgroup T_d and possesses $3N - 6 = 9$ fundamental vibrations. The fundamental mode $\nu_1(a_1)$ at 2186.87 cm^{-1} is not degenerated, $\nu_2(e)$ at 970.97 cm^{-1} is twofold, and $\nu_3(f_2)$ at 2189.19 cm^{-1} and $\nu_4(f_2)$ at 913.47 cm^{-1} are threefold degenerated.

3.1 Linear absorption

In case of linear absorption, the absorption coefficient for silane at the frequency position ν is determined by the line shape profile $P_{SiH_4}(\nu, \nu_{SiH_4})$ and the line strength $S(\nu)$, which depend on the transition under consideration:

$$\alpha'(\nu) = \frac{\ln\left(\frac{I_0}{I(\nu)}\right)}{pd} = S(\nu) P_{SiH_4}(\nu, \nu_{SiH_4}). \tag{4}$$

Here, $\nu_{SiH_4} = 944.213$ cm^{-1} belongs to the vibrational–rotational transition of the silane molecule in the R branch of the ν_4 fundamental mode [13], having only a spectral distance of $\Delta_{AE} := \nu_{CO_2} - \nu_{SiH_4} = 0.015$ cm^{-1} (450 MHz) from the $10P(20)$ laser line. Then, the absorption coefficient α' for the total absorption is obtained by integration of $\alpha'(\nu)$ over the spectral distribution of the incoming laser light:

$$\alpha' = \int_0^{+\infty} P_{Laser}(\nu)\alpha'(\nu)\, d\nu. \tag{5}$$

According to [14], the absorption line has a full Doppler width $\Delta_{D,SiH_4} = 62.1$ MHz at room temperature, and the Lorentz width of the line can be calculated by means of

$$\Delta_{L,SiH_4} = \beta 3.08\,\text{GHz}\frac{(p/\text{kPa})^\delta}{\sqrt{T/\text{K}}} = \beta 177.8\,\text{MHz}(p/\text{kPa})^\delta, \tag{6}$$

where β and δ are still free parameters of order one. Because the laser line is very narrow-banded, the spectral

emission profile of the laser in (5) can be approximated by a δ function:

$$\alpha' \approx \int_0^{+\infty} \delta(\nu - \nu_{CO_2})\alpha'(\nu)\mathrm{d}\nu$$

$$= \alpha'(\nu_{CO_2}) = S(\nu_{CO_2})\, P_{SiH_4}(\nu_{CO_2}, \nu_{SiH_4}). \quad (7)$$

The resulting normalized Voigt profile of the absorption line can be written as

$$P_{SiH_4}(\nu_{CO_2}, \nu_{SiH_4}) = 2\sqrt{\frac{\ln 2}{\pi}}\frac{1}{\Delta_{D,SiH_4}}\left(\frac{A}{\pi}\int_{-\infty}^{+\infty}\frac{\exp(-x^2)\mathrm{d}x}{A^2 + (B-x)^2}\right) \quad (8)$$

with

$$A = A(p) = \frac{\Delta_{L\ SiH_4}(p)}{\Delta_{D,SiH_4}}\sqrt{\ln 2} \quad (9)$$

and

$$B = B(\Delta_{AE}) = \frac{\Delta_{AE}}{\Delta_{D,SiH_4}} 2\sqrt{\ln 2}. \quad (10)$$

The convolution integral in (8) reduces to

$$\int_{-\infty}^{+\infty}\frac{\exp(-x^2)\mathrm{d}x}{A^2 + (B-x)^2} \approx \frac{\sqrt{\pi}}{A^2 + B^2}, \quad (11)$$

because the contribution of the Voigt profile at the spectral position of the emission line is dominated by the Lorentz component. Therefore, we have:

$$\alpha' = \alpha'(p;\beta,\delta) = \frac{2S(\nu_{CO_2})}{\pi\Delta_{L,SiH_4}(p)}\frac{1}{1 + \left(\frac{2\Delta_{AE}}{\Delta_{L,SiH_4}(p)}\right)^2}. \quad (12)$$

If additionally a non-resonant contribution α_0 is considered, one obtains for the total absorption coefficient α:

$$\alpha := \alpha' + \alpha_0. \quad (13)$$

A comparison with experimental data by Haggerty and Cannon [4] for the absorption of CO_2 laser radiation at the $10P(20)$ line by silane shows that for $\beta = 1.25$ and $\delta = 1.6$ in (6) and $\alpha_0 = 0.35 \times 10^{-2}\ \mathrm{Pa^{-1}\,m^{-1}}$, the theoretical curve

$$\alpha(p) = \left(\frac{7.78(p/\mathrm{kPa})^{-1.6}}{1 + 16.4(p/\mathrm{kPa})^{-3.2}} + 0.35\right) \times 10^{-2}\ \mathrm{Pa^{-1}\,m^{-1}} \quad (14)$$

fits the experimental data in a satisfying manner. In Fig. 7, the experimental and theoretical curve are shown to prove this result. Obviously, the absorption measured by Haggerty and Cannon can be explained by the absorption of a single silane molecule in the vibrational ground state under the influence of its self-broadening. In our experiments with high spectral energy density of the light source, a different absorption behaviour could be stated, as given in Fig. 2. In the following section, a model is introduced which elucidates the differences between the two measurements.

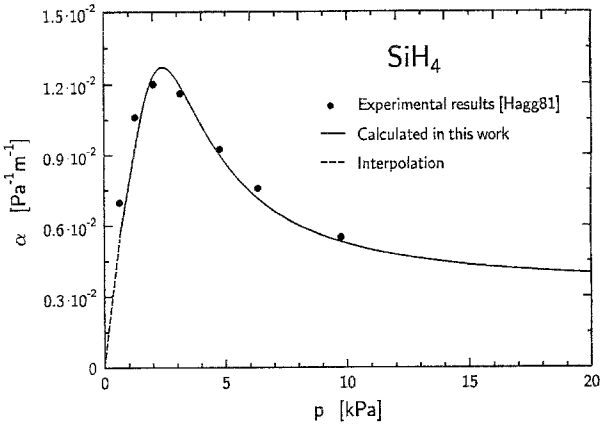

Fig. 7. Pressure dependence of the absorption coefficient α for silane vs pressure p at the $10P(20)$ laser line and low spectral energy density $\varrho_{Ph} = 10^{-12}\ \mathrm{J\,s\,m^{-3}}$

3.2 *Rate-equation model*

The mechanism discussed in detail in section 3.1 describing the absorption of CO_2 laser radiation by silane does not take into account any intermolecular transfer of absorbed energy between the silane molecules, but only the intramolecular radiative transition between the vibrational ground state and the first excited state. In the following, a rate-equation model for the absorption is presented which besides radiation processes also allows homomolecular vibrational–vibrational (V–V) and vibrational–translational (V–T) collisions as possible pathways of energy transfer between the excited molecules. In particular for silane, the V–V processes are very efficient [15, 16].

3.2.1 Assumptions. The absorption model is based on the following assumptions:

- Only vibrational states up to $v_4 = 3$ are considered and only transitions between neighboured vibrational states, $\Delta v_4 = \pm 1$, are allowed.
- Intramolecular energy transfer to other fundamental modes is neglected.
- The rotational levels within one vibrational state are not considered.
- A constant gas temperature of $T = 300$ K is assumed.
- Diffusion processes are neglected.
- The following relaxation and excitation mechanisms are included:

  (*i*) Absorption of laser photons between the vibrational ground level and the first excited level of the fundamental mode $v_4(f_2)$ (Sect. 3.1):

  $$SiH_4(v_4 = 0) + h\nu \rightarrow SiH_4(v_4 = 1). \quad (15)$$

  Due to the anharmonicities of the molecular potential, absorption of laser photons by vibrationally

excited molecules is unlike [15]. The height of absorption is ruled by the Einstein coefficient B_{01}.

(*ii*) Spontaneous emission

$$SiH_4(v_4 = 1) \rightarrow SiH_4(v_4 = 0) + h\nu, \tag{16}$$

ruled by the transition probability A_{10}.

(*iii*) Induced emission

$$SiH_4(v_4 = 1) + h\nu \rightarrow SiH_4(v_4 = 0) + 2h\nu, \tag{17}$$

ruled by the Einstein coefficient B_{10}.

(*iv*) For the adequate description of the pressure-dependent absorption discussed in Sect. 3.1, the absorption profile according to (4) and (14) is taken into account within the corresponding terms for absorption and induced emission of the rate equations. The introduction of particle densities instead of partial pressures is useful for the modelling; therefore, instead of $P_{SiH_4}(v_{CO_2}, v_{SiH_4}, p)$ the corresponding line profile $P(n) := P_{SiH_4}(v_{CO_2}, v_{SiH_4}, n)$ is taken.

(*v*) Energy transfer by means of intramolecular V–V collisions:

$$SiH_4(v_4 = 1) + SiH_4(v_4 = 1) \underset{K^{(-)}_{1,1;0,2}}{\overset{K^{(+)}_{1,1;0,2}}{\rightleftharpoons}} SiH_4(v_4 = 0) + SiH_4(v_4 = 2) + \Delta E_{1,1;0,2} \tag{18}$$

$$SiH_4(v_4 = 1) + SiH_4(v_4 = 2) \underset{K^{(-)}_{1,2;0,3}}{\overset{K^{(+)}_{1,2;0,3}}{\rightleftharpoons}} SiH_4(v_4 = 0) + SiH_4(v_4 = 3) + \Delta E_{1,2;0,3} \tag{19}$$

$$SiH_4(v_4 = 2) + SiH_4(v_4 = 2) \underset{K^{(-)}_{2,2;1,3}}{\overset{K^{(+)}_{2,2;1,3}}{\rightleftharpoons}} SiH_4(v_4 = 1) + SiH_4(v_4 = 3) + \Delta E_{2,2;1,3}. \tag{20}$$

The energy difference $\Delta E_{n,m;u,v}$ is released by the collision. If $E(v_4 = n)$ is the energy of the n-fold excited vibrational level, e.g., the relation $\Delta E_{1,1;0,2} = E(v_4 = 1) + E(v_4 = 1) - [E(v_4 = 0) + E(v_4 = 2)]$ holds. In the case of the harmonic oscillator with equidistant energy levels, $\Delta E_{1,1;0,2} = 0$, as well as the two other energy differences considered here. As a result of anharmonicities in the molecular potential, the differences between adjacent vibrational energy levels are usually decreasing for the higher vibrational states, and the values for $\Delta E_{n,m;u,v}$ are not zero. In the model discussed here, they are considered equal: $\Delta E_{VV} := \Delta E_{1,1;0,2} = \Delta E_{1,2;0,3} = \Delta E_{2,2;1,3}$. For ΔE_{VV}, a value of 10.48 cm^{-1} is employed in the following because it is rather small compared to the thermal energy (208.36 cm^{-1}). If the harmonic oscillator is assumed, the rate coefficients for the V–V collisions fulfill the requirement of detailed balancing, which means for the general reaction

$$A(v_4 = n) + A(v_4 = m) \underset{K^{(-)}_{n,m;n-1,m+1}}{\overset{K^{(+)}_{n,m;n-1,m+1}}{\rightleftharpoons}} A(v_4 = n - 1) + A(v_4 = m + 1)$$

a relation

$$K^{(+)}_{n,m;n-1,m+1} = n(m + 1)K^{(+)}_{1,0;0,1}. \tag{21}$$

For the collisional processes considered here, one obtains:

$$K^{(+)}_{1,1,;0,2} = 2K, \quad K^{(+)}_{1,2;0,3} = 3K, \quad K^{(+)}_{2,2;1,3} = 6K, \tag{22}$$

where the definition $K := K^{(+)}_{1,0;0,1}$ is used.

In the case of local thermal equilibrium at a gas temperature T, the rate coefficients $K^{(+)}$ and $K^{(-)}$ are related to each other by the Boltzmann factor:

$$\frac{K^{(-)}}{K^{(+)}} = \exp\left(-\frac{\Delta E_{VV}}{k_B T}\right) =: \beta_{VV}. \tag{23}$$

(*vi*) Energy transfer by means of intramolecular vibrational–translational collisions:

$$SiH_4(v_4 = 1) \underset{M^{(-)}_{1;0}}{\overset{M^{(+)}_{1;0}}{\rightleftharpoons}} SiH_4(v_4 = 0) + \Delta E_{1;0}, \tag{24}$$

$$SiH_4(v_4 = 2) \underset{M^{(-)}_{2;1}}{\overset{M^{(+)}_{2;1}}{\rightleftharpoons}} SiH_4(v_4 = 1) + \Delta E_{2;1}, \tag{25}$$

$$SiH_4(v_4 = 3) \underset{M^{(-)}_{3;2}}{\overset{M^{(+)}_{3;2}}{\rightleftharpoons}} SiH_4(v_4 = 2) + \Delta E_{3;2}. \tag{26}$$

The difference between the first vibrationally excited level and the vibrational ground level is calculated to be $\Delta E_{1;0} = E(v_4 = 1) - E(v_4 = 0) = h\nu_{SiH_4} = 944.213$ cm^{-1}. In the model considered here, the energy levels of the vibrational states are equidistant as mentioned before, which means: $\Delta E_{VT} := 944.213\ cm^{-1} = h\nu_{SiH_4} = \Delta E_{1;0} = \Delta E_{2;1} = \Delta E_{3;2}$. As for the V–V collisions, a relation among the rate coefficients for V–T collisions is valid in the approximation of the harmonic oscillator:

$$A(v_4 = n) \underset{M^{(-)}_{n;n-1}}{\overset{M^{(+)}_{n;n-1}}{\rightleftharpoons}} A(v_4 = n - 1),$$

$$M^{(+)}_{n;n-1} = nM^{(+)}_{1;0}. \tag{27}$$

For the collisional processes considered, this leads to:

$$M^{(+)}_{1;0} = 1M, \quad M^{(+)}_{2;1} = 2M, \quad M^{(+)}_{3;2} = 3M, \tag{28}$$

where the definition $M := M^{(+)}_{1;0}$ is used.

The detailed balance gives (as before) the relation among the rate coefficients $M^{(+)}$ and $M^{(-)}$:

$$\frac{M^{(-)}}{M^{(+)}} = \exp\left(-\frac{\Delta E_{VT}}{k_B T}\right) =: \beta_{VT}. \tag{29}$$

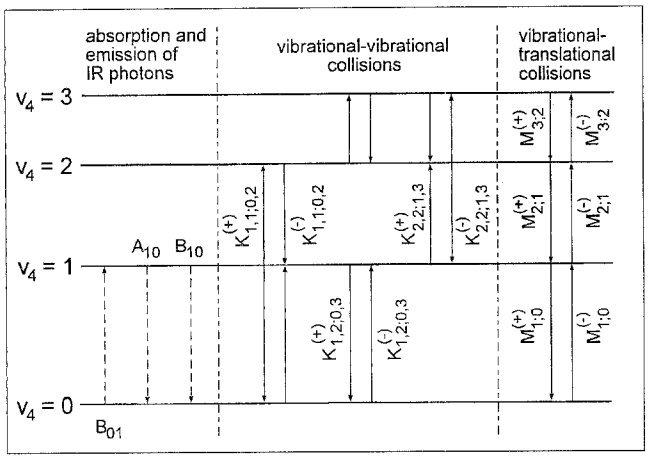

Fig. 8. Energy transfer processes considered in the kinetic model

A survey of the processes taken into account by the absorption model is given in Fig. 8.

3.2.2 Rate equations. The population density of the vibrational levels $v_4 = 0, 1, 2, 3$ (Fig. 8) follows from a rate-equation system which balances the processes discussed before and is applied here to the stationary case. As a result, one obtains the four rate equations for the population densities n_0, n_1, n_2, and n_3 of the different vibrational states $v_4 = 0,1,2,3$ from the relations:

$$0 \overset{!}{=} \frac{dn_0}{dt} = -\varrho_{Ph} B_{01} n_0 P(n) + A_{10} n_1 + \varrho_{Ph} B_{10} n_1 P(n) + K[2(n_1^2 - \beta_{VV} n_0 n_2) + 3(n_1 n_2 - \beta_{VV} n_0 n_3)] + M[(n_1 - \beta_{VT} n_0)], \tag{30}$$

$$0 \overset{!}{=} \frac{dn_1}{dt} = +\varrho_{Ph} B_{01} n_0 P(n) - A_{10} n_1 - \varrho_{Ph} B_{10} n_1 P(n) + K[-4(n_1^2 - \beta_{VV} n_0 n_2) - 3(n_1 n_2 - \beta_{VV} n_0 n_3) + 6(n_2^2 - \beta_{VV} n_1 n_3)] + M[-(n_1 - \beta_{VT} n_0) + 2(n_2 - \beta_{VT} n_1)], \tag{31}$$

$$0 \overset{!}{=} \frac{dn_2}{dt} = +K[2(n_1^2 - \beta_{VV} n_0 n_2) - 3(n_1 n_2 - \beta_{VV} n_0 n_3) - 12(n_2^2 - \beta_{VV} n_1 n_3)] + M[-2(n_2 - \beta_{VT} n_1) + 3(n_3 - \beta_{VT} n_2)], \tag{32}$$

$$0 \overset{!}{=} \frac{dn_3}{dt} = +K[3(n_1 n_2 - \beta_{VV} n_0 n_3) + 6(n_2^2 - \beta_{VV} n_1 n_3)] + M[-3(n_3 - \beta_{VT} n_2)]. \tag{33}$$

From (33), one obtains

$$n_3 = n_3(n_0, n_1, n_2; x). \tag{34}$$

Here, $\underline{\kappa} := (n, K, M, \beta_{VV}, \beta_{VT}, B_{01}, B_{10}, A_{10})$ is the general set of constants for the rate-equation system. Introducing the total particle number density n and the equation

$$n_0 = n - (n_1 + n_2 + n_3), \tag{35}$$

one can see by insertion into (34) that n_3 merely depends on n_1 and n_2:

$$n_3 = n_3(n_1, n_2; \underline{\kappa}). \tag{36}$$

According to (35), also n_0 depends only on n_1 and n_2:

$$n_0 = n_0(n_1, n_2; \underline{\kappa}). \tag{37}$$

After insertion of (37) and (36) into the nonlinear equation system (30–33), the solutions

$$n_1 = n_1(\varrho_{Ph}; \underline{\kappa}) \tag{38}$$

and

$$n_2 = n_2(\varrho_{Ph}; \underline{\kappa}) \tag{39}$$

follow.

Finally, the variation of the spectral energy density along the axis of the absorption chamber is given by the photon balance equation

$$\frac{d\varrho_{Ph}}{dx} = -\sigma_{01} P(n) \left(n_0 - \frac{B_{10}}{B_{01}} n_1 \right) \varrho_{Ph}, \tag{40}$$

with the molecular absorption cross section σ_{01}.

3.2.3 Results of the model. At first, all parameters required to solve the set of rate equations are gathered. Refering to (3), the spectral energy density of the laser at the entrance of the absorption chamber is about 10^{-10} Jsm^{-3} (Tab. 1). As transition probability A_{10} for spontaneous emission, the value of the CO molecule is representatively taken, which is in the range of $10\ s^{-1}$. The Einstein coefficient B_{10} for induced emission can be calculated to be

$$B_{10} = \frac{\lambda^3}{8\pi h} A_{10} = 7 \times 10^{17}\ m^3 J^{-1} s^{-2}, \tag{41}$$

where h is Planck's constant and λ the laser wavelength. Because the v_4 fundamental vibration of silane is threefold degenerated, the Einstein coefficient B_{01} for absorption is

$$B_{01} = 3B_{10} = 2 \times 10^{18}\ m^3 J^{-1} s^{-2}. \tag{42}$$

Following the ideal gas equation at room temperature, the population densities n_v for the pressure range 0–20 kPa are between 0 and $4.8 \times 10^{24}\ m^{-3}$.

The magnitude of the Boltzmann factor β_{VV} (23) is dominated by the energy difference ΔE_{VV}. With $\Delta E_{VV} = 10.48\ cm^{-1}$, one gets $\beta_{VV} = 0.95$, which means that the rate coefficients for the back and the forth reaction differ only by 5%. Considerably smaller is the factor β_{VT} for the vibrational–translational collisions (29). For room temperature, a value $\beta_{VT} = 10^{-2}$ is typical, using $\Delta E_{VT} = 944.213\ cm^{-1}$.

In contrast to molecules like CO and CO_2, which play important roles in laser discharges [17, 18] and are therefore the object of intensive research, no data for silane are known to the authors, as far as the rate coefficients K (vibrational–vibrational collision) and M (vibrational–translational collision) are concerned. Measured rate coefficients for a CO–CH_4 system and the pressure regime discussed here have magnitudes of $K = 5 \times 10^{-20}\ m^3\,s^{-1}$ and $M = 10^4\ s^{-1}$ [19]. Compared to the heteromolecular CO–CH_4 system, V–V transfer occurs much faster in the case of the homomolecular silane system because it is fully resonant. Moreover, the silane molecule reaches the Vibrational Quasi Continuum (VQC) already at moderate excitation ($v_4 > 3$) [20]. The VQC is characterized by very dense energy levels. The mentioned effects are considered in the modelling by a factor $K = 5 \times 10^{-17}\ m^3\,s^{-1}$, which is three orders of magnitude higher than that of the CO–CH_4 system. In a similar way, the vibrational–translational coefficient is assumed to have a rather high value of $M = 10^7\ s^{-1}$, so that now the set of constants $\underline{\kappa} := (n, K, M, \beta_{VV}, \beta_{VT}, B_{01}, B_{10}, A_{10})$ is fixed.

The modelling was performed with *Mathematica* for *Windows*. At first, the numerical program calculates an interpolation table for n_1 and n_2 as function of the spectral energy density ϱ_{Ph} and determines [according to (37)] the population density n_0 of the vibrational ground state $v_4 = 0$. In a last step, the differential equation (40) is solved stepwise by numerical methods within the interval $0 \le x \le d$.

A first result of the model is the dependence of the spectral energy density on the absorption length for $p = 20$ kPa. In Fig. 9, ϱ_{Ph} is shown for a starting value of $\varrho_{Ph} = 10^{-12}\ Jsm^{-3}$, which corresponds to the case investigated by Haggerty and Cannon [4], and for $\varrho_{Ph} = 10^{-10}\ Jsm^{-3}$, which is characteristic for the laser employed in this work. The constant slope in the semilogarithmic plot valid for the low spectral energy density reflects the fact that the absorption can be described by the integral Lambert-Beer law :

$$\varrho_{Ph}(x) = \varrho_{Ph}(x = 0)\,e^{-\alpha p x}. \qquad (43)$$

Assuming a 100 times higher spectral energy density ($\varrho_{Ph} = 10^{-10}\ J\,s\,m^{-3}$), the model yields quite different results. Now, the spectral energy density can no longer be described by the integral Lambert Beer law in (43). In this case, the absorption coefficient α is only defined locally when preceding along the axis of the absorption chamber.

The population density distributions are strongly depending upon the spectral energy density, as shown in Fig. 10. At low spectral energy density, a substantial deviation of the population densities of excited states from the thermal equilibrium state for 300 K occurs only at the entrance of the absorption chamber. In contrast to that, a high spectral energy density has a strong influence on the population of the vibrational states of the molecule leading to a distribution which deviates from thermal equilibrium. When the spectral energy density diminishes to a value where the population densities of the vibrational states are in the vicinity of thermal equilibrium, the local absorption behaviour can be expressed by the integral Lambert-Beer law.

Corresponding hypothetical vibrational population temperatures T_v of the excited states $v = 1, 2, 3$ exposed to a radiation field are calculated from the population densities by using the following equation:

$$T(v) = \frac{\Delta E_{VT}}{k_B \cdot \left[\ln\left(\frac{n_{v-1}}{n_v}\right) + \ln\left(\frac{G_v}{G_{v-1}}\right)\right]}, \qquad v = 1, 2, 3, \qquad (44)$$

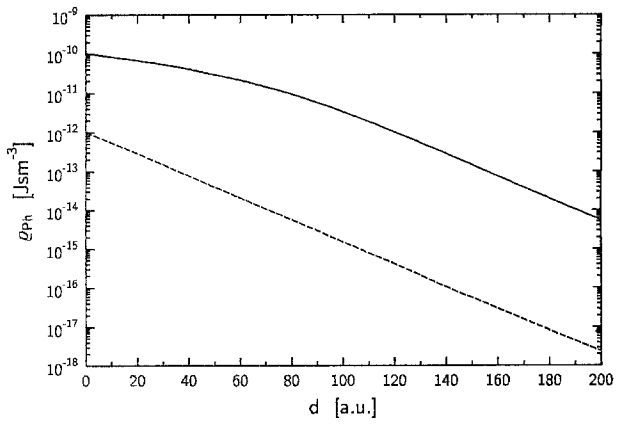

Fig. 9. Calculated spectral energy density ϱ_{Ph} with beam entrance values of $\varrho_{Ph} = 10^{-12}\ J\,s\,m^{-3}$ (---) and $\varrho_{Ph} = 10^{-10}\ J\,s\,m^{-3}$ (—) vs absorption length d

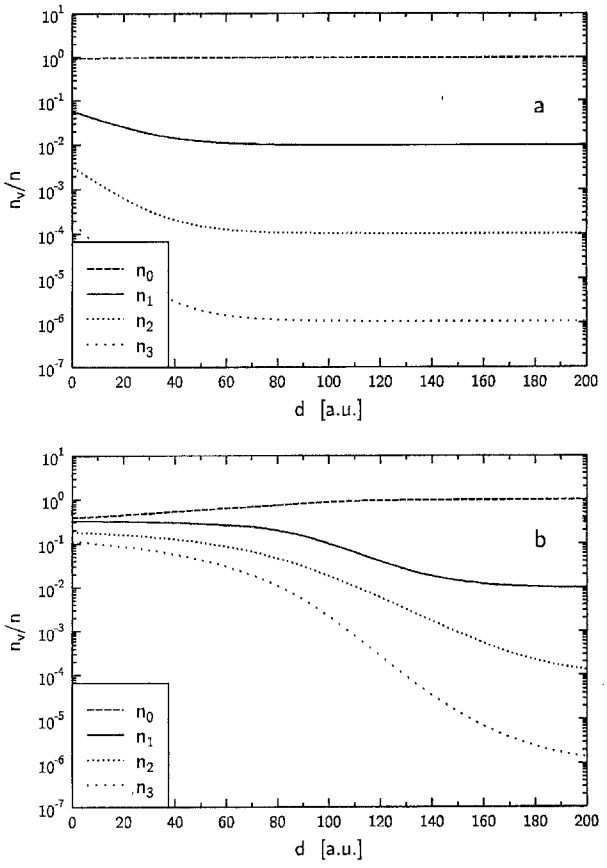

Fig. 10a,b. Calculated relative population densities n_v/n with beam entrance values of (**a**) $\varrho_{Ph} = 10^{-12}\ J\,s\,m^{-3}$ and (**b**) $\varrho_{Ph} = 10^{-10}\ J\,s\,m^{-3}$ vs absorption length d

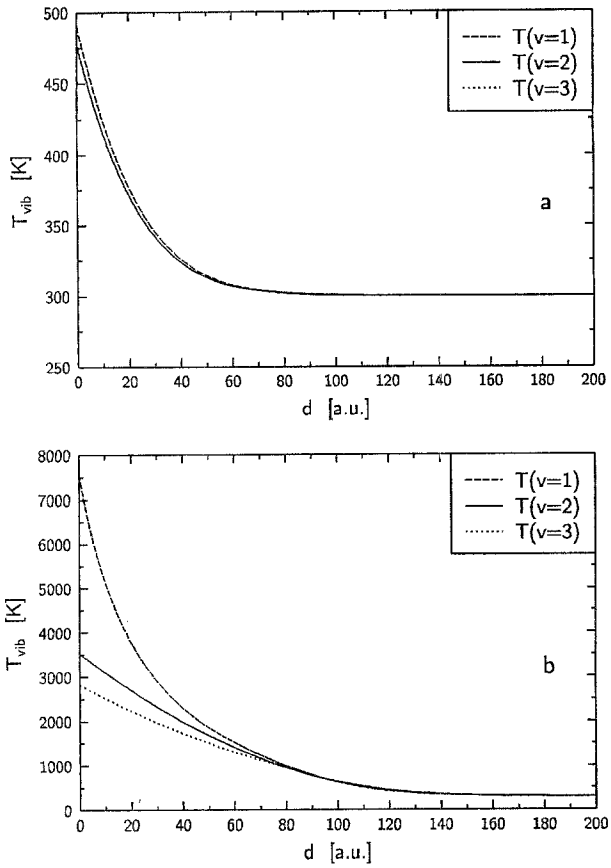

Fig. 11a,b. Calculated vibrational temperatures T_{vib} with beam entrance values of (**a**) $\varrho_{Ph} = 10^{-12}\,J\,s\,m^{-3}$ and (**b**) $\varrho_{Ph} = 10^{-10}\,J\,s\,m^{-3}$ vs absorption length d

where $G_v = \frac{1}{2}(v+1)(v+2)$ is the degeneracy factor for a three-fold degenerate vibration excited by v quanta [21]. The results are given in Fig. 11. Notice that at low spectral energy density, the calculated vibrational temperatures are nearly independent of the considered state. Starting with the highest value of 403 K for the third excited state at the entrance of the absorption chamber, the vibrational temperatures decrease exponentially to the gas temperature (300 K). For a given absorption length, all vibrational states are in thermal equilibrium among each other, characterized by a temperature T, the latter having its maximum at the entrance of the absorption chamber. This means that the energy transfer processes are able to distribute the absorbed laser energy from the first excited state to all vibrational states involved, according to the Boltzmann factor.

The situation alters when the spectral energy density is 100 times higher. Especially at the entrance of the absorption chamber, the formally defined vibrational temperatures are quite different, as can be seen from Fig. 11. For the model considered here, they grow up to 1370 K for the third excited state. This can be explained on one hand by the raised population of the first excited state due to the high absorption rate of laser photons. Another reason is an efficient energy transfer to the residual states together with negligible vibrational–translational relaxation rates. With decreasing spectral energy density, when preceding

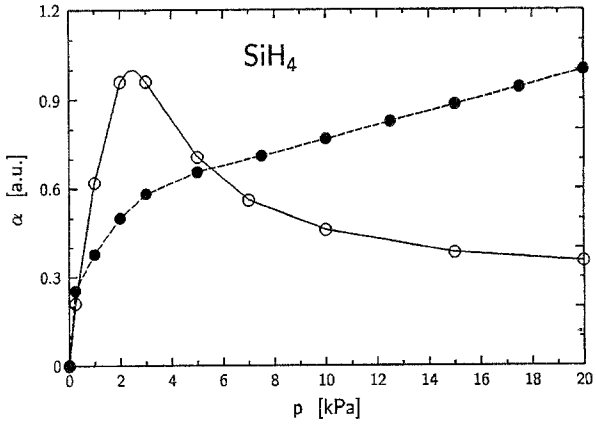

Fig. 12. Calculated absorption coefficient α vs silane pressure p, evaluated for $d = 20$ cm and for $\varrho_{Ph} = 10^{-12}\,J\,s\,m^{-3}$ (○) and $\varrho_{Ph} = 10^{-10}\,J\,s\,m^{-3}$ (●)

along the absorption cell, the different vibrational temperatures converge and finally reach the gas temperature, similarly to the low-spectral-energy-density case.

The pressure dependence of the absorption coefficient

$$\alpha = \text{const} \times \frac{\ln\left(\dfrac{\varrho_{Ph}(x=0)}{\varrho_{Ph}(x=d)}\right)}{p}, \tag{45}$$

for a fixed absorption length $d = 20$ and a low spectral energy density, is shown in Fig. 12, which is in a good agreement with the measurements of Haggerty and Cannon (Fig. 7). Figure 12 shows also the pressure dependence of the absorption coefficient for a high spectral energy density. The plot describes qualitatively the absorption behaviour measured here (Fig 2), where in contrast to the low-energy-density case the absorption coefficient does not decrease with increasing pressure after reaching a maximum. Nevertheless, it should be mentioned that in the case of a high spectral energy density, the absorption coefficient is averaged over the absorption length due to the deviation from the integral Lambert-Beer law (Fig. 9). The latter effect takes place if the spectral energy density of the laser light used for the absorption measurements is high enough to disturb significantly the thermal population of the vibrational states. Then, the vibrational–vibrational and vibrational–translational collisions are no longer able to distribute the whole absorbed radiation energy over the vibrational states involved according to the Boltzmann factor. The rate-equation model presented here describes in a satisfying way both the pressure dependence of the absorption coefficient for silane measured in this work and the silane absorption data given in literature. It could be shown that the measured absorption behaviour depends critically on the magnitude of the spectral energy density of the laser employed.

4 Conclusion

Absorption measurements on the gases silane, ammonia, acetylene, and the silane/argon and silane/diborane

mixtures, which are important for ultrafine powder production, were performed in the spectral range of the CO_2 laser from 9.2 to 10.8 μm and in the pressure range 0–100 kPa. In agreement with already published data, the measurements confirmed that for the $10P(20)$ laser line, silane has the strongest absorption of all gases investigated here. Within the accessible parameter range, the highest absorption coefficient measured for silane was $\alpha = (3.25 \pm 0.33) \times 10^{-2}$ $Pa^{-1}m^{-1}$ at a pressure of 20 kPa. For SiH_4, the pressure dependence of the absorption coefficient observed in this work differs significantly from the measurements of Haggerty and Cannon [4]. The rate-equation model introduced in this work made it possible to explain this absorption behaviour by the high spectral energy density of the CO_2 laser employed here. For ammonia, the measured absorption behaviour on the $10P(20)$ laser line agrees with literature. The absorption coefficient is considerably lower than that of silane and reaches $(4.5 \pm 0.8) \times 10^{-4}$ $Pa^{-1}m^{-1}$ at 20 kPa. Its maximum is observed at the $10R(6)$ laser line (7×10^{-3} $Pa^{-1}m^{-1}$ at $p = 2.5$ kPa).

In comparison to silane, the absorption coefficient of acetylene and diborane is rather low ($\leq 2.1 \times 10^{-5}$ $Pa^{-1}m^{-1}$ for acetylene).

Measurements on silane/argon mixtures demonstrate that for the proper choice of appropriate reactant gas mixtures with respect to the application for the pyrolysis process, it is not sufficient to use absorption data of the pure gases. Besides the spectral energy density (average laser power), the IR absorption of silane at the $10P(20)$ laser line depends also strongly on the composition of the gas under investigation.

Acknowledgements. The authors wish to thank P. Buchner and Dr. K. Oerding for fruitful discussions concerning the solution of the rate equations. This work was partially supported by the Land Nordrhein-Westfalen under contract number Az.: IV A1–213 013 92-.

References

1. J. Förster, M.v. Hoesslin, J.H. Schäfer, J. Uhlenbusch, W. Viöl: In *Proc. 10th Int'l Symp. on Plasma Chemistry*, ed. by U. Ehlemann, H.G. Lergon, K. Wiesemann, **1**, 1.4-23p1-1.4-23p6, Bochum, Germany (1991) paper 1.4–23
2. J. Förster, M.v. Hoesslin, J.H. Schäfer, J. Uhlenbusch: In *Proc. 11th Int'l Symp. on Plasma Chemistry*, ed. by J. Harry, Loughborough, UK (1993) pp. 1739–1744
3. M.v. Hoesslin, J. Förster, J.H. Schäfer, J. Uhlenbusch: Appl. Phys. B **61**, 367 (1995)
4. J.S. Haggerty, W.R. Cannon: In *Laser Induced Chemical Processes*, ed. by J.I. Steinfeld (Plenum, New York, 1981) Chap. 3, pp. 165–241
5. R.R. Patty, G.M. Russwurm, W.A. McClenny, D.R. Morgan: Appl. Opt. **13**, 2850 (1974)
6. R.C. Lord, E. Nielsen: J. Chem. Phys. **19**, 1 (1951)
7. W.J. Lehmann, C.O. Wilson, I. Shapiro: J. Chem. Phys. **28**, 781 (1958)
8. I.N. Knyazev, N.P. Kuzmina, V.S. Letokhov, V.V. Lobko, A.A. Sarkisyan: Appl. Phys. **22**, 429 (1980)
9. R.V. Ambartzumian, N.P. Furzikov, Yu.A. Gorokhov, V.S. Letokhov, G.N. Makarov, A.A. Puretzkii: Opt. Commun. **18**, 517 (1976)
10. E.M. Alonso, R.J. Angelo, E.J. Quel: Appl. Phys. B **47**, 233 (1988)
11. M.L. Azcarate, E.J. Quel: Appl. Phys. B **47**, 223 (1988)
12. M. Snels, R. Larciprete, R. Fantoni, E. Borsella, A. Giardini-Guidoni: Chem. Phys. Lett. **122**, 480 (1985)
13. J.W.C. Johns, W.A. Kreiner, J. Susskind: J. Mol. Spectrosc. **60**, 400 (1976).
14. J. Förster: Laserchemische Erzengung, Charakterisierung und Verdichtung ultrafeiner SiC- und SiC/B-Pulver. Dissertation, Heinrich-Heine-Universität Düsseldorf, Germany (1995)
15. H. Stafast: Appl. Phys. A **45**, 93 (1988)
16. W. Fuß: Private communications, Max-Planck Institut für Quantenoptik, München, Germany (1994)
17. K. Smith, J.K. Thomson: *Computer Modelling of Gas Lasers* (Plenum, New York 1978)
18. T. Doerk, J. Ehlbeck, P. Jauernik, J. Stanco, J. Uhlenbusch, T. Wottka: J. Phys. D. **26**, 1015 (1993)
19. E.A. Gregory, M.M. Maricq, R.M. Siddles, C.T. Wickham-Jones, C.J.S.M. Simpson: J. Chem. Phys. **78(6)**, 3881 (1983)
20. M.v. Hoesslin: Aufbauener Box-CARS-Diagnostik zur Messung von räumlichen Dichte- und Temperatur profilen in einer laser induzierten chemischen Reaktionszone. Dissertation, Heinrich-Heine-Universität Düsseldorf, Germany (1993)
21. G. Herzberg: *Molecular Spectra and Molecular Structure. II. Infrared and Raman Spectra of Polyatomic Molecules*, (Van Nostrand Reinhold, New York 1944) p. 81